Right Ventricular Strain Analysis from 3D Echocardiography by Using Temporally Diffeomorphic Motion Estimation

Zhijun Zhang[1], David J. Sahn[1,2], and Xubo Song[1]

[1] Department of Biomedical Engineering
[2] Department of Pediatric Cardiology, Oregon Health and Science University
20000 NW Walker Road, Beaverton, OR 97006, USA
{zhangzhi,songx,sahn}@ohsu.edu

Abstract. Quantitative motion analysis of the right ventricle (RV) is important to study its function. However, the RV study is more difficult than that of left ventricle (LV) because of its complex shape and the limitations of the existing imaging methods. We propose a diffeomorphic motion estimation method and apply it to the 3D echocardiography of five open-chest pigs under different steady states. We first validate the motion estimation method by using sonomicrometry. Then we estimate the myocardium strain of different steady states. The RV free wall (RVFW) is divided into twelve segments and their strain patterns in each steady states together with the corresponding cardiac mechanics are analyzed. This is the first time to quantitatively analyze the RVFW segment strains from 3D echocardiography by using algorithm.

Keywords: Right ventricle, strain analysis, motion estimation, diffeomorphic registration.

1 Introduction

Studying the right ventricle (RV) function is very important to understand the mechanism of pulmonary hypertension, cardiomyopathy, congenital heart disease and biventricular relation. RV motion is used as an indicator of the RV function. Cardiac imaging is widely used for noninvasive study of the RV motion. Although large amount of quantitative motion analysis on the left ventricle (LV) have been reported, studies of RV mostly focus on qualitative analysis [1–3]. Quantitatively study of the RV is more difficult because of its irregular shape, trabeculate structure in endocardium and thin myocardium in the images. Among the few works on RV motion estimation, all used MR images. Young *et al.* [5] proposed a finite element based method to track the mid myocardium surface motion from tagged MR images. Harber *et al.* [4] used a volumetric finite element model to analyze the 3D motion of the myocardium from tagged MR images. Zhang *et al.* [6] proposed a combined active shape and appearance model based method to track the motion from MR images. We use echocardiography for the RV motion analysis because of

S. Ourselin, D. Rueckert, and N. Smith (Eds.): FIMH 2013, LNCS 7945, pp. 474–482, 2013.

its advantages of realtime imaging, high resolution and low cost. We apply a temporally smooth diffeomorphic registration method for the RV strain analysis. It has three advantages than the above model based methods. First, the method is an intensity based method in which the displacement at each voxel is estimated with subvoxel accuracy. Second, the estimated transformation is topology preserving which is physically plausible for cardiac motion analysis. Third, the motion analysis is independent of the RV shape. Once the cardiac motion is estimated, the transformation can be used to analyze the strain on any point given the strain directions on it. We first validated the accuracy of motion estimation method by using sonomicrometry. Then we applied the method to echocardiography sequences under different steady states including baseline, RV pacing, RV apex pacing and RV outflow tract (RVOT) pacing. The RV free wall (RVFW) was divided into 12 segments and the averaged segment strains were analyzed. We present the difference of the average segment strains in each steady states and analyze the myocardium mechanics involved. As our knowledge, it is the first time that 3D echocardiography is used to estimate the RVFW strain by algorithm.

2 Method

2.1 Diffeomorphic Motion Estimation

We propose a diffeomorphic registration based motion estimation method. The deformation between any two consecutive frames is defined by a diffeomorphism and the deformation between any two frames is the composition of the diffeomorphisms between them. The diffeomorphism is defined by its velocity field with a differential equation of $\frac{d\boldsymbol{\phi}}{dt} = \boldsymbol{v}(\boldsymbol{\phi}(\boldsymbol{x},t),t), \boldsymbol{\phi}(\boldsymbol{x},0) = \boldsymbol{x}$, with $t \in [0,T], (\boldsymbol{x} \in \Omega \subset R^3)$ and $T = N_s - 1$ where N_s being the number of frames. The motion estimation problem is stated as an optimization of a variational energy of the velocity field $\boldsymbol{v}(\boldsymbol{x},t)$:

$$\hat{\boldsymbol{v}} = arg \inf_{\boldsymbol{v} \in V} \lambda \int_0^T ||\boldsymbol{v}(\boldsymbol{x},t)||_V^2 dt + \sum_{n=1}^{n=T} E_{SSD}(I_{n-1}(\boldsymbol{x}), I_n(\boldsymbol{\phi}_{n-1,n})), \tag{1}$$

with the first term a regularizer to evaluate the spatiotemporal smoothness and the second term a similarity measurement which evaluates the summed squared difference (SSD) of the voxel intensity between I_{n-1} and the unwarped frame $I_n(\boldsymbol{\phi}_{n-1,n})$, with $\boldsymbol{\phi}_{n-1,n}$ being the deformation between two frames. The regularization term is defined as weighted sum of a spatial and a temporal regularization term:

$$||\boldsymbol{v}||_V^2 = \int_\Omega \sum_{i,j=1,2,3} (\frac{\partial^2 v_j}{\partial {x_i}^2})^2 d\boldsymbol{x} + w_t |\frac{\partial \boldsymbol{v}}{\partial t}|^2 d\boldsymbol{x}, \tag{2}$$

with the first term measuring the spatial gradient of the velocity field, and the second term temporal gradient of the velocity field. Optimization of Eqn.(1) searches a spatiotemporal smooth function which minimizes the summed SSD similarity between all consecutive frames.

The optimization is solved by numerical method. We use a parameterized function form for velocity field [8, 9]. It is discretized temporally into a series of 3D B-spline functions at time $t_k(k = 0, 1, ..., N_t, t_k = k\Delta t, \Delta t = 1/N_f)$, with N_f being the number of time steps between two consecutive frames, $N_t = N_f * (N_s - 1)$ being the total number of B-spline functions. The B-spline function at time point t_k is defined as $\boldsymbol{v}(\boldsymbol{x}, t_k) = \sum \mathbf{c}_{m;k}\boldsymbol{\beta}(\boldsymbol{x} - \boldsymbol{x}_m)$, with $\mathbf{c}_{m;k}$ being the control vectors located on a uniform grid of $\boldsymbol{x}_m$ at t_k, $\boldsymbol{\beta}(\boldsymbol{x} - \boldsymbol{x}_m)$ being the 3D B-spline kernel function at $\boldsymbol{x}_m$ which is the tensor product of the 1-D B-spline functions. Then $\boldsymbol{\phi}(\boldsymbol{x}, t)$ can be expressed as the forward Euler integral of velocity field $\boldsymbol{v}(\boldsymbol{x}, t)$ by assuming that the velocity of each point is piecewisely constant within a time step. The transformation $\boldsymbol{\phi}_{0,t_k}$ is related with $\boldsymbol{\phi}_{0,t_{k-1}}$ by:

$$\boldsymbol{\phi}_{0,t_k} = \boldsymbol{\phi}_{0,t_{k-1}} + \boldsymbol{v}(\boldsymbol{\phi}_{0,t_{k-1}}, t_{k-1})\Delta t = (\mathbf{Id} + \boldsymbol{v}_{k-1}\Delta t) \circ \boldsymbol{\phi}_{0,t_{k-1}}, \tag{3}$$

with $\mathbf{Id}$ the identity transformation and $\boldsymbol{v}_{t_k} = \boldsymbol{v}(\boldsymbol{x}, t_k)$ the velocity field at t_k. The transformation $\boldsymbol{\phi}_{n-1,n}$ is then denoted by composition of all the small deformation under the velocity field between time $t_{(n-1)*N_f}$ and t_{n*N_f}:

$$\boldsymbol{\phi}_{n,n-1} = \prod_{(n-1)N_s}^{nN_s-1} (\mathbf{Id} + \boldsymbol{v}_k) \tag{4}$$

By using Eqn.(4), each SSD term in Eqn.(1) is only related to the velocity field parameters within the time of consecutive frames, so the derivative of the SSD with respect to the velocity field can be evaluated independently. The temporal regularization term regularizes the velocity field globally.

We use a steepest descent method to optimize the Eqn.(1). The explicit estimation of the derivative of the energy function with respect to the B-spline parameters can be referred to [8, 9].

2.2 Strain Analysis

We use Green strain [10] in our study and the strain tensor is defined by:

$$\boldsymbol{\epsilon} = \frac{1}{2}(\boldsymbol{F}\boldsymbol{F}^{\boldsymbol{T}} - \boldsymbol{I}), \tag{5}$$

with $\boldsymbol{F}$ being the matrix of the transformation gradient and $\boldsymbol{I}$ the 3×3 identity matrix. The normal strain is estimated by projecting the strain tensor to any direction $\boldsymbol{d}$ by equation:

$$E_{\boldsymbol{d}} = \boldsymbol{d}^T \boldsymbol{\epsilon} \boldsymbol{d}. \tag{6}$$

In our study, the strains are evaluated at each point along the radial, circumferential and longitudinal directions.

3 Datasets and Experiment

We validate the motion estimation method by using 3D echocardiography sequences of five open-chest pigs under steady states of baseline, RV pacing, RV

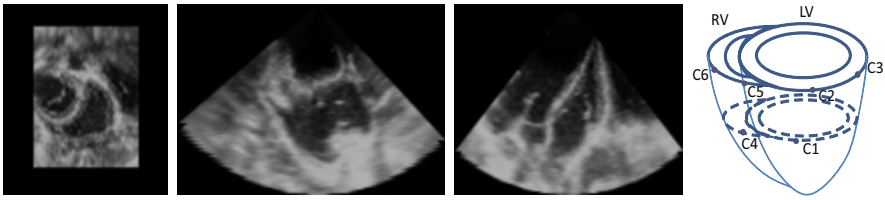

Fig. 1. The axial, sagittal and coronal views of an example ED frame and the sonomicrometers positions in the myocardium

apex pacing and RV outflow tract (RVOT) pacing. Different pacings were created by connecting a bipolar pacer lead to different pacing sites. The images are acquired with a Philips IE33 system. A typical baseline sequence has 30 frames with frame size $151 \times 129 \times 101$. The end-diastolic (ED) frame of this sequence is shown in Fig.(1) as an example.

We first validate the RV motion estimation method by using sonomicrometry. We implanted six sonomicrometers in the myocardium of one pig, the position of the sono crystals are shown in Fig.(1). Then four pairs of points distance (C2-C4, C2-C5, C4-C5 and C5-C6) varying with time are recorded in the sonomicrometry. We then compare the two points peak strain which is defined as the ratio of the maximum relative shortening with the initial distance with the sonomicrometry used as ground truth.

Then we evaluate the strain on RV endocardium in all the four steady states. The variance of the strain patterns in different steady states and the cardiac mechanics are analyzed. The RV endocardium in the ED frame is segmented by using a semiautomatic method. The image sequences are reformated so that the images are in the right hand system and the RV short axis planes are parallel with the xy plane. We first label the contours of the RV endocardium in each short axis views by using closed B-spline curves. We manually pick some points along the RV endocardium wall and then a fixed number of points are uniformly sampled on each contours (see Fig.(2)). A triangle mesh is then generated by connecting points in each two neighbor contours anticlockwisely. In order to analyze the RVFW strain in detail, the RVFW is divided horizontally as inferior, inferiorlateral, anteriorlateral and anterior (1,2,3,4) and vertically as apical, mid and basal (1,2,3) segments. The RVFW are divided into 12 segments with S1 standing for the apical inferior segment and S12 standing for the basal anterior segments for example (see Fig.(2)). The local cardiac system is defined at each of the triangle mesh vertex. The radial direction $\boldsymbol{d}_r$ of a vertex is defined as the averaged normal direction of the triangles which are joint at it. We define the normal direction of short axis planes as $\boldsymbol{n}_{sa}$, the circumferential direction $\boldsymbol{d}_c$ is defined as the cross-product of $\boldsymbol{n}_{sa}$ with $\boldsymbol{d}_r$, and the longitudinal direction is defined as the cross-product of $\boldsymbol{d}_c$ with $\boldsymbol{d}_r$. We illustrate the cardiac coordinate system in Fig.(2) and the bottom row of this figure shows the three orthogonal directions in an example RV mesh.

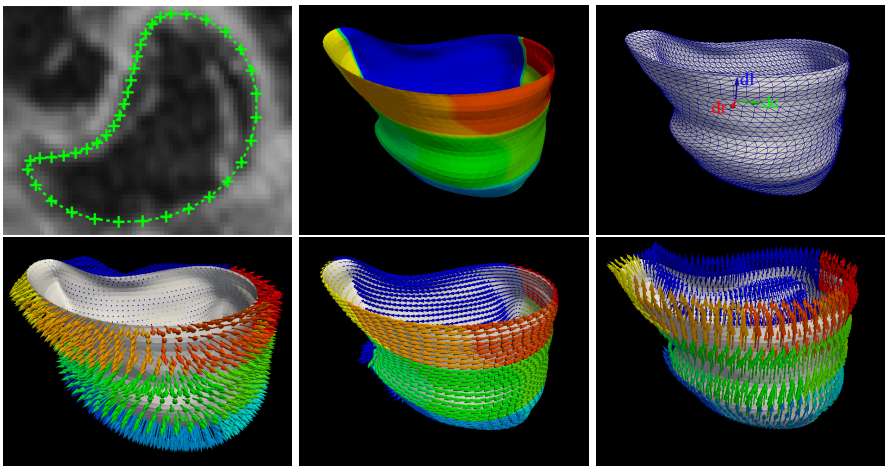

Fig. 2. The cardiac coordinate system in our experiments. The left top figure shows the endocardium contour. The mid top figure shows the 12 endocardium segments in colors. The top right figure shows the direction of d_r,d_c and d_l in a vertex of the endocardium. The bottom row shows the d_r,d_c and d_l directions in all the mesh vertices.

4 Results

We first show the result of the sonomicrometry validation in Fig.(3). The left figure in Fig.(3) shows the scatter plot of the 16 peak strains estimated from our method and from the sonomicrometry. The correlation between the peak strain is 0.86 which means very consistent result with the ground truth. The middle and the right plots shows the two points strain curves in one cardiac cycle in sonomicrometry and in our methods. We can see the curves are very similar, the correlations of the sono strain curve with the echo strain curve are 0.91 and 0.92 in these two pairs of points. This shows that our method has good temporal consistency with the ground truth.

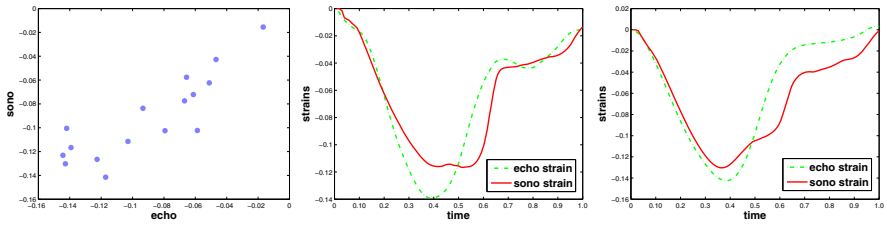

Fig. 3. The result from the sonomicrometry validation. Left figure shows the two point peak strains estimated from the sono and echo. The mid and right plots shows the correlation between the sono and echo two points strains.

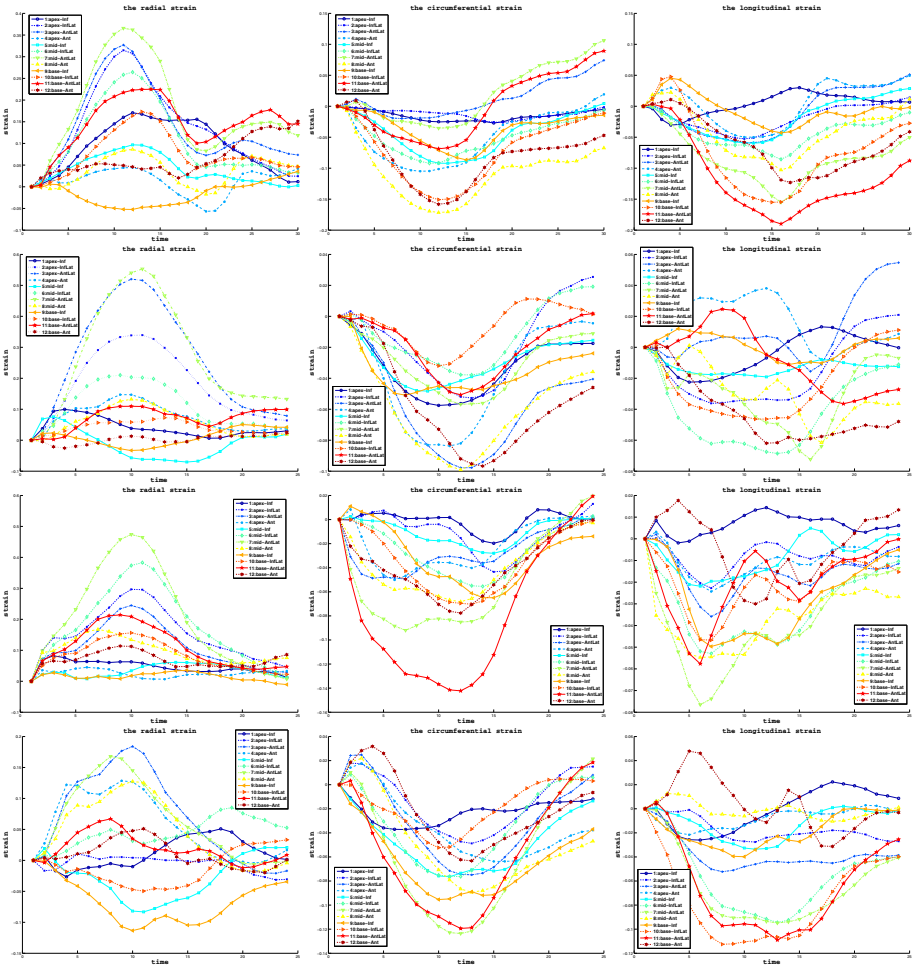

Fig. 4. From top to bottom, it shows the RS, CS and LS of a same pig under baseline, RV pacing, RV apex pacing and RVOT pacing steady states

We got similar strain patterns for the five pigs under different steady states and we use one pig to show its strain pattern variation in different steady states. We show the strain curves of one cardiac cycle of four steady states in Fig.(4). The corresponding end-systolic (ES) strains on RVFW are shown in Fig.(5) with colormap and the values of the ES strain and their average in apical, mid and basal segments are listed in table.(1). The first row shows the three normal strains of the baseline. We can see nearly all of the segments reaches optimum simultaneously. The time that LS strain reaches minimum is different than those of the RS and CS. The RS magnitude decreases in order of apical, mid and basal segments. The magnitude of CS decreases in order of basal, mid and apical segments. The side three segments near the RVOT (S4,S8,S12) have larger CS

than other segments. This means the circumferential shorting is larger in the RVOT area. The LS decreases with order of basal, mid and apical segments. It means that longitudinal shortening is dominant in basal segments and radial elongation is dominant in apical segments.

The second row in Fig.(4) shows the strains in RV pacing. We can see after RV pacing the average RS in apical and mid segments increases, and that in the basal segments decreases. The radial elongation is more dominant in the lateral segments (S3,S7,S11) than baseline. For CS, apical segments the largest average. The average of LS decreases in apical, mid and basal segments.

The third row in Fig.(4) shows the strains in the RV apex pacing. The average RS in mid segments is larger than the baseline. The RS is also more dominant in the lateral segments than baseline. The average LS strain in apical, mid and basal segments is smaller than baseline. We can see that the LS of all segments reaches minimum early than that of the baseline.

The fourth row in Fig.(4) shows the strains in the RVOT pacing. The average RS in apical, mid and basal segments is much smaller than baseline. The region near vertical side segments opposite to RVOT (S1,S5,S9,S10) has negative RS and the vertical segments near RVOT (S3,S4,S7,S8,S11,S12) has positive RS, and two lateral segments (S2, S6) has very small RS. That means RS are dominant in the segments in RVOT region. The average CS of the mid segments are larger than those of apical and basal segments. The average of LS in apical, mid and basal segments are all smaller than baseline. The minimum of LS reaches earlier than the baseline but later than that of RV apex pacing.

Table 1. The ES strains in the four steady states. S1 to S12 are the RVFW segments, $\bar{M}_{apx}$,$\bar{M}_{mid}$ and $\bar{M}_{bas}$ are the mean strain of the apical, mid and basal segments, and BSL, RV, RVA, RVOT are baseline, RV pacing, RV apex pacing, RVOT pacing respectively. For each state, the three rows are values for radial, circumferential and longitudinal stains.

States	Apex					Mid					Base				
	S1	S2	S3	S4	M_{apx}	S5	S6	S7	S8	M_{mid}	S9	S10	S11	S12	M_{bas}
BSL	0.17	0.31	0.31	0.04	0.21	0.10	0.26	0.36	0.09	0.20	0.01	0.16	0.22	0.05	0.1
	-0.02	-0.01	-0.02	-0.1	-0.04	-0.09	-0.09	-0.04	-0.17	-0.10	-0.07	-0.15	-0.07	-0.16	-0.11
	-0.02	-0.03	-0.04	-0.04	-0.02	-0.05	-0.09	-0.15	-0.10	-0.10	-0.04	-0.15	-0.19	-0.12	-0.13
RVP	0.03	0.33	0.49	0.14	0.25	0.01	0.19	0.54	0.14	0.21	0.01	0.04	0.12	0.02	0.03
	-0.06	-0.05	-0.10	-0.09	-0.08	-0.04	-0.05	-0.06	-0.10	-0.06	-0.05	-0.04	-0.5	-0.09	-0.05
	-0.01	-0.04	-0.01	-0.04	-0.02	-0.02	-0.07	-0.07	-0.04	-0.05	-0.01	-0.04	-0.01	-0.06	-0.03
RVA	0.06	0.30	0.23	0.01	0.15	0.05	0.38	0.45	0.12	0.25	0.02	0.16	0.20	0.10	0.12
	-0.01	-0.01	-0.03	-0.04	-0.02	-0.02	-0.05	-0.09	-0.07	-0.06	-0.05	-0.08	-0.15	-0.08	-0.06
	-0.01	-0.01	-0.01	-0.01	-0.01	-0.02	-0.05	-0.05	-0.05	-0.04	-0.05	-0.04	-0.02	-0.03	-0.04
RVOT	-0.01	0.01	0.18	0.13	0.08	-0.08	0.03	0.15	0.13	0.06	-0.11	-0.05	0.03	0.05	-0.02
	-0.03	-0.04	-0.06	-0.04	-0.04	-0.08	-0.08	-0.12	-0.07	-0.08	-0.10	-0.05	-0.11	-0.05	-0.08
	-0.01	-0.03	-0.05	-0.01	-0.03	-0.03	-0.09	-0.09	-0.01	-0.05	-0.04	-0.11	-0.10	-0.01	-0.06

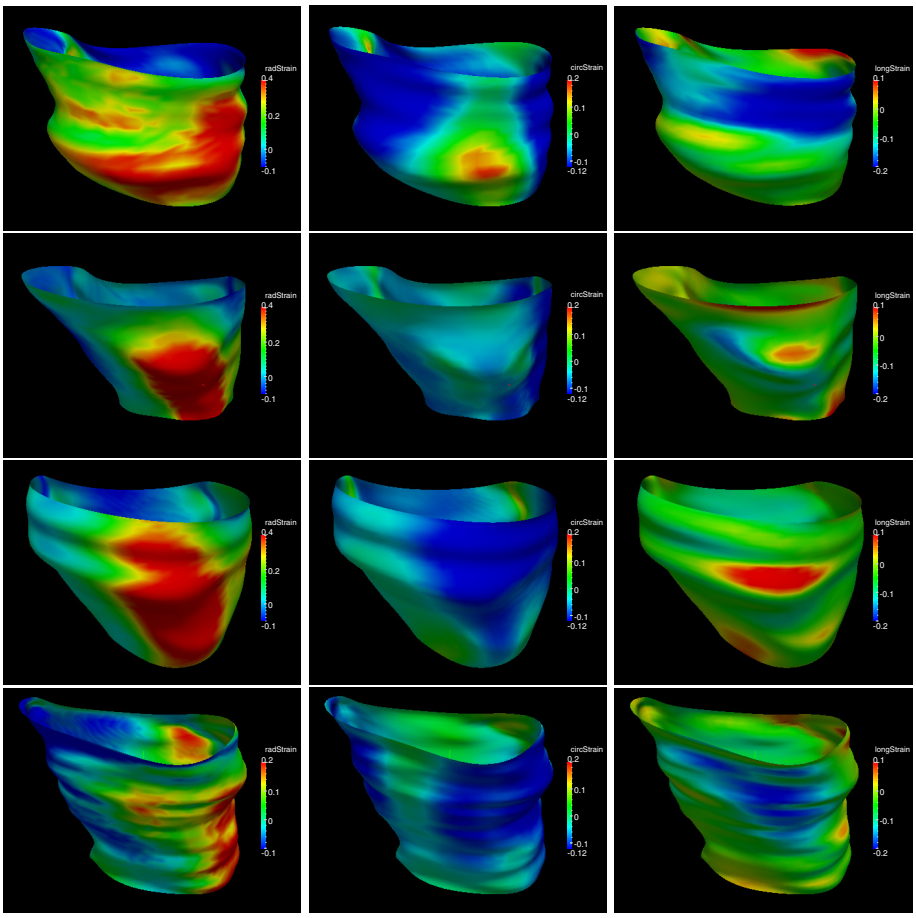

Fig. 5. The ES frame strain color plot on the RVFW in baseline, RV pacing, RV apex pacing and RVOT pacing

5 Conclusion

In this paper, we validate a diffeomorphic motion estimation method with echocardiography. The results from the sonomicrometry show that our methods has good consistency with the ground truth. We applied the method to the RVFW strain analysis of the different steady states. Different segment strain patterns were found and possible reasons are analyzed. Results show that our method is a promising tool for RV Analysis.

Acknowledgement. This paper is supported by a NIH/NHLBI grant 1R01HL102407-01 awarded to Xubo Song and David Sahn.

References

1. Mertens, L.L., Friedberg, M.K.: Imaging the right ventricle — current state of art. Nat. Rev. Cardiol. 7(10), 551–563 (2010)
2. Haddad, F., Hunt, S.A., Rosenthal, D.N., Murphy, D.J.: Right Ventricular Function in Cardiovascular Disease, Part I: Anatomy, Physiology, Aging, and Functional Assessment of the Right Ventricle. Circulation 117, 1436–1448 (2008)
3. Ho, S.Y., Nihoyannopoulos, P.: Anatomy, echocardiography, and normal right ventricular dimensions. Heart, 92(S1) 2–13 (2006)
4. Haber, I., Metaxas, D.N., Axel, L.: Three-dimensional motion reconstruction and analysis of the right ventricle using tagged MRI. Med. Imag. Anal. 4(4), 335–355 (2000)
5. Young, A.A., Fayad, Z.A., Axel, L.: Right ventricular midwall surface motion and deformation using magnetic resonance tagging. Am. J. Physiol. 271(6P2) 2677–2688 (1996)
6. Zhang, H.H., Wahle, A., Johnson, R.K., Scholz, T.D., Sonka, M.: 4-D Cardiac MR Image Analysis: Left and Right Ventricular Morphology and Function. IEEE Trans. Med. Imag. 29(2), 350–364 (2010)
7. Meunier, J.: Tissue motion assessment from 3D echographic speckle tracking. Phys. Med. Biol. 43, 1241–1254 (1998)
8. Craene, M.D., Piella, G., Camaraa, O., Duchateaua, N., Silvae, E., Doltrae, A., D'hooge, J., Brugadae, J., Sitgese, M., Frangi, A.F.: Temporal diffeomorphic free-form deformation: application to motion and strain estimation from 3D echocardiography. Med. Imag. Anal. 16(1), 427–450 (2012)
9. Ashburner, J.: A fast diffeomorphic image registration algorithm. NeuroImage 38(1), 95–113 (2007)
10. Fung, Y.C.: First Course in Continuum Mechanics. Springer (2010)